Global Biogeochemical Cycles

Supporting Information for

Sensitivity of ozone dry deposition to ecosystem-atmosphere interactions: A critical appraisal of observations and simulations

Meiyun Lin[1,2]*, Sergey Malyshev[2], Elena Shevliakova[2], Fabien Paulot[1,2], Larry W. Horowitz[2], Silvano Fares[3], Teis N. Mikkelsen[4], Leiming Zhang[5]

[1]Program in Atmospheric and Oceanic Sciences, Princeton University, Princeton, NJ 08540, USA
[2]NOAA Geophysical Fluid Dynamics Laboratory, Princeton, NJ 08540, USA
[3]Council for Agricultural Research and Economics, Research Centre for Forestry and Wood, Arezzo, Italy
[4]Department of Environmental Engineering, Technical University of Denmark, 2800 Kgs. Lyngby, Denmark
[5]Air Quality Research Division, Science and Technology Branch, Environment and Climate Change Canada, Toronto, Canada

* Corresponding author: M. Lin (Meiyun.Lin@noaa.gov)

Contents of this file

Text S1. Influence of snow cover on wintertime surface ozone simulations

We modify the input parameters for non-stomatal deposition to simulate more realistic $V_{d,O3}$ and surface O_3 over snow-cover landscapes and under cold temperatures (**Figs. S1 and S2**). In LM4.0, ground and cuticular resistances to snow (R_{snow}) surfaces are given a value of 2000 s m^{-1} for O_3 and dry cuticular resistances (R_{cutd}) are increased by as much as two times their original values when temperatures are below -1° C, using the formula: R_{cutd} ($T < -1°$ C) = $R_{cutd}\ e^{0.2(-1-T)}$ (Zhang et al., 2003). LM4.0 with these parameters simulates wintertime $V_{d,O3}$ values of 0.10-0.25 cm s^{-1} over snow-covered landscapes, which are on the upper end of the typical observed values (0-0.2 cm s^{-1}) (Helmig et al., 2007; Helmig et al., 2012; Wu et al., 2016). AM4 with $V_{d,O3}$ from LM4.0 underestimates surface O_3 during winter over snow-covered landscapes north of 45°N. We thus increase R_{snow} from 2000 to 10000 s m^{-1} and increase R_{cutd} to an upper limit of 3 times the original value when temperatures are below −1° C. With these adjusted parameters, wintertime $V_{d,O3}$ in the northern high latitudes decrease to 0.05-0.1 cm s^{-1} in LM4.0 (**Fig.S2),** leading to improved wintertime surface O_3 simulations in these regions compared to the original scheme

(**Fig.S1**). Wintertime $V_{d,O3}$ in the adjusted scheme for LM4.0 generally agree with observations from European boreal forests (**Fig.2** in the main text).

Text S2. Land model spin-up

Both the LM3.0 and LM4,0 experiments consist of a 300-yr potential vegetation spin-up phase (i.e., undisturbed by human activity), an intermediate land use spin-up phase (1700-1860), and a historical phase (1861-2014). In the 300-yr potential vegetation spin-up phase, atmospheric forcings were constructed by cycling 10 times through the historical data (Sheffield et al., 2006) for 1948-77, atmospheric CO_2 concentration was set to the preindustrial level (286 ppm) and vegetation disturbances by land use were not applied. The purpose of this stage is to obtain realistic natural vegetation state (including vegetation biomasses, vegetation types, phenology, and physical characteristics of land surface such as roughness length and others) before starting application of land use changes. In the intermediate spin-up phase, land use disturbances (Hurtt et al., 2011) and harvesting were applied and run for 161 years from 1700-1860. The purpose of this stage is to generate realistic land use state by the beginning of historical simulation; since the model keeps track of age structure of secondary vegetation tiles, it is important to let them reach consistency with the sequence of the land use transitions and absorb the shock of initial land use application (Sentman et al., 2011). When a historical land-use scenario is instantaneously applied, the land experiences an abrupt change in state, as the vegetation undergoes a transition from the potential state to the state prescribed by the land use scenario at that particular time. The instantaneous cutting of natural forests due to transitions to croplands, pastures, and secondary vegetation results in a drastic change in the carbon stocks and other vegetation properties through deforestation and logging. This is referred to as the "shock of initial land use" (Sentman et al., 2011). Following these initial transitions, the secondary vegetation needs time to regrow, which is essential for producing appropriate vegetation state, including carbon stocks, biomasses, and vegetation properties (Sentman et al., 2011). Finally, in the historical (1861-2014) phase, historical CO_2 concentrations were prescribed and land use disturbances and harvesting continued to be applied.

Text S3. Calculation of stomatal contribution

The stomatal deposition (G_s) is the ratio of the effective stomatal conductance to the overall surface conductance weighted by the deposition velocity.

$$G_s = (1/R_s)/(1/R_s+1/R_{ns})*V_d$$

Where R_s is the effective resistance associated with stomata, which reflects the change in stomatal conductance and the change in conductance that leads to stomata associated with aerodynamic and quasi-laminar resistances. R_{ns} is the effective non-stomatal resistance, and V_d is the deposition velocity.

Helmig, D., L. Ganzeveld, T. Butler, & S. J. Oltmans (2007), The role of ozone atmosphere-snow gas exchange on polar, boundary-layer tropospheric ozone - a review and sensitivity analysis, Atmos. Chem. Phys., 7, doi: 10.5194/acp-7-15-2007.

Helmig, D., P. Boylan, B. Johnson, S. Oltmans, C. Fairall, R. Staebler, et al. (2012), Ozone dynamics and snow-atmosphere exchanges during ozone depletion events at Barrow, Alaska, J. Geophys. Res.-Atmos., 117, doi: 10.1029/2012jd017531.

Hurtt, G. C., L. P. Chini, S. Frolking, R. A. Betts, J. Feddema, G. Fischer, et al. (2011), Harmonization of land-use scenarios for the period 1500-2100: 600 years of global gridded annual land-use transitions, wood harvest, and resulting secondary lands, Climatic Change, 109(1-2), 117-161, doi: 10.1007/s10584-011-0153-2.

Sentman, L. T., E. Shevliakova, R. J. Stouffer, & S. Malyshev (2011), Time Scales of Terrestrial Carbon Response Related to Land-Use Application: Implications for Initializing an Earth System Model, Earth Interact, 15, doi: Artn 30 10.1175/2011ei401.1.

Sheffield, J., G. Goteti, & E. F. Wood (2006), Development of a 50-year high-resolution global dataset of meteorological forcings for land surface modeling, J. Clim., 19(13), 3088-3111, doi: 10.1175/Jcli3790.1.

Wu, Z. Y., R. Staebler, R. Vet, & L. M. Zhang (2016), Dry deposition of O3 and SO2 estimated from gradient measurements above a temperate mixed forest, Environ. Pollut., 210, 202-210, doi: 10.1016/j.envpol.2015.11.052.

Zhang, L. M., J. R. Brook, & R. Vet (2003), A revised parameterization for gaseous dry deposition in air-quality models, Atmos. Chem. Phys., 3, 2067-2082, doi: 10.5194/acp-3-2067-2003.

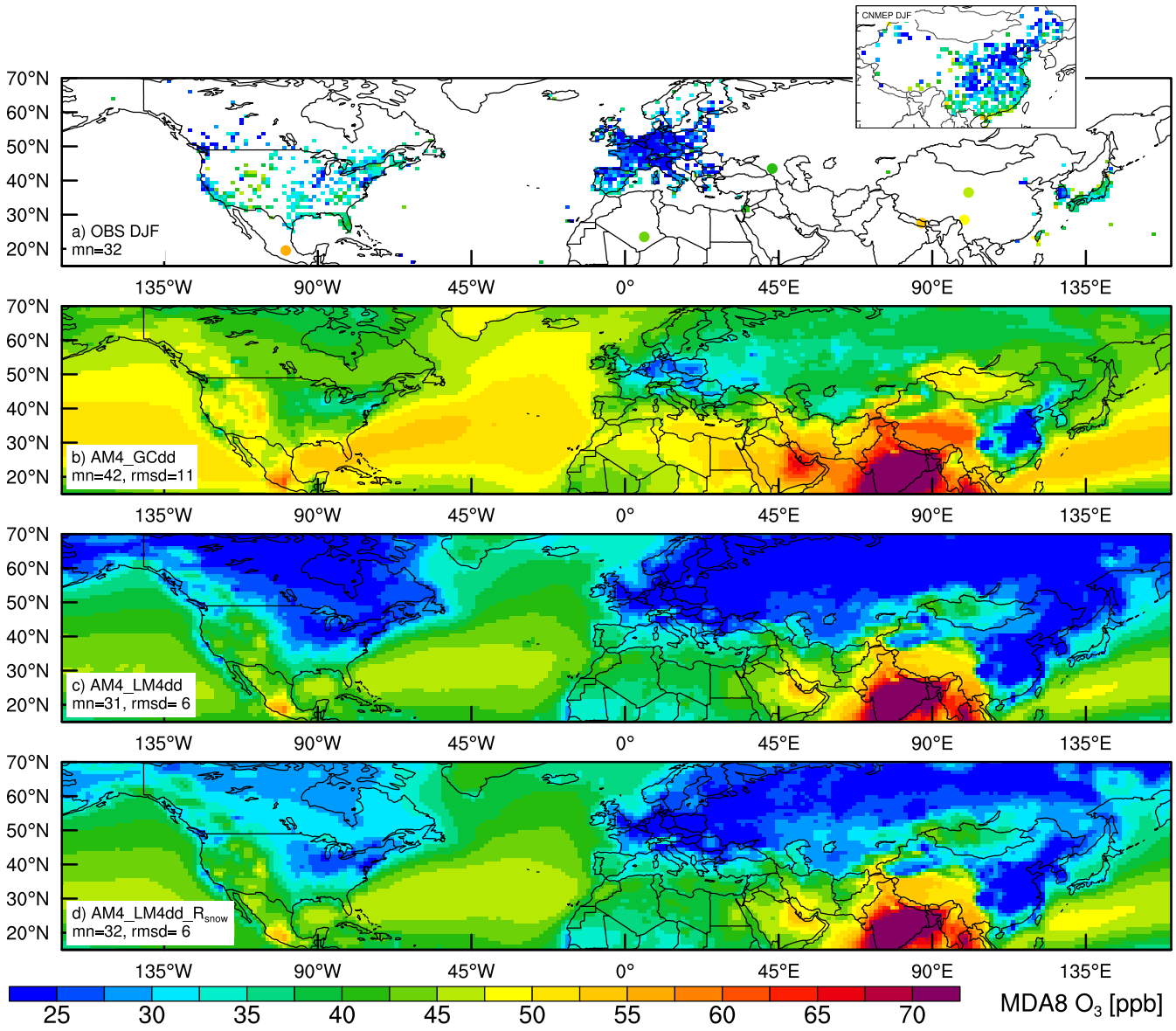

Figure S1. DJF mean MDA8 O_3 mixing ratios from TOAR observations (a; inset map for CNMEP data) and AM4 simulations (2005-2014) with $V_{d,O3}$ from the Wesely scheme as implemented in GEOS-Chem (b), GFDL-LM4.0 with non-stomatal parameterization as in the Zhang scheme (c), and GFDL-LM4.0 with slower deposition over snow and under cold temperatures (d, see Text S1 for details).

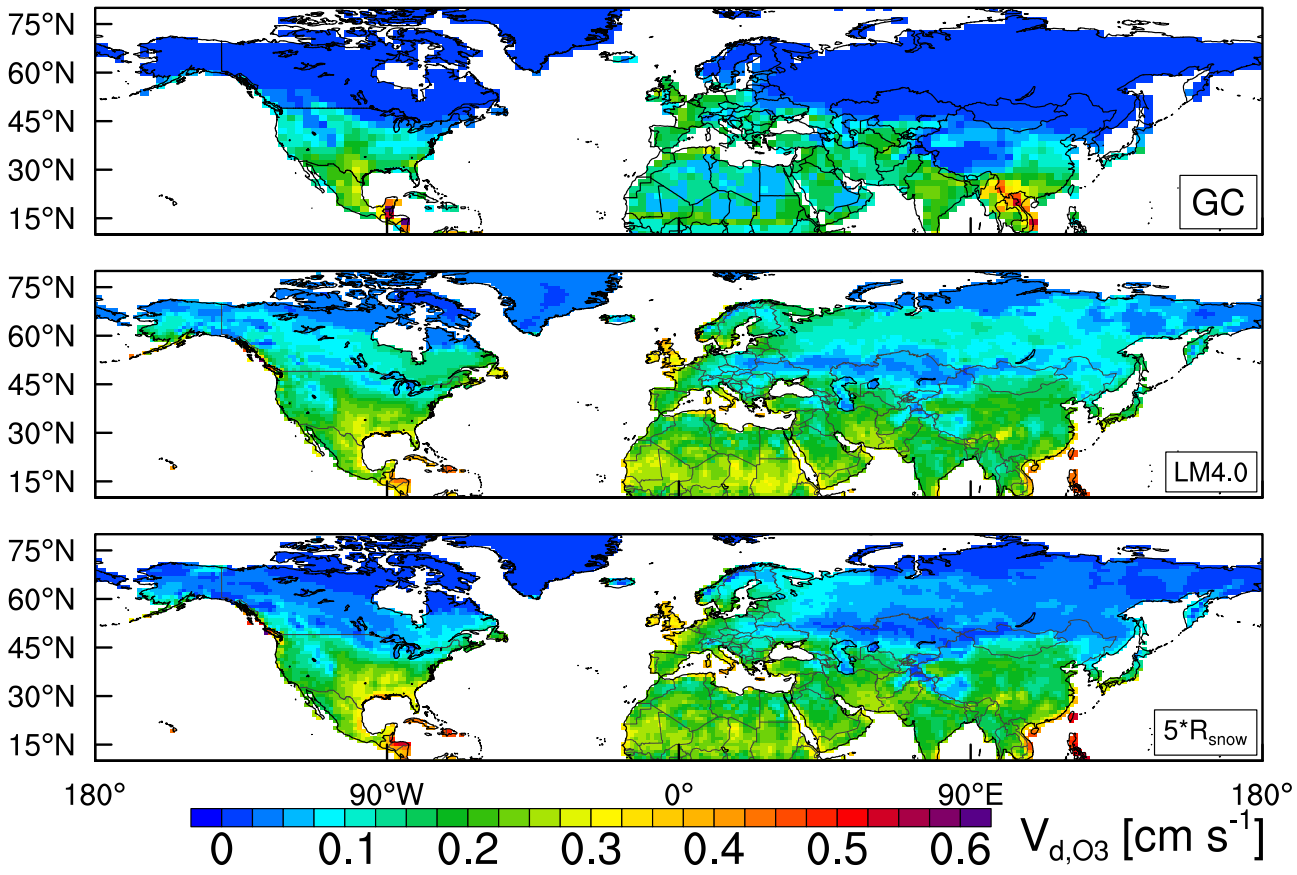

Figure S2. DJF mean $V_{d,O3}$ from GEOS-Chem, LM4.0, and LM4.0 with greater ground resistance over snow. Shown are the 10-yr average from 2005 to 2014.

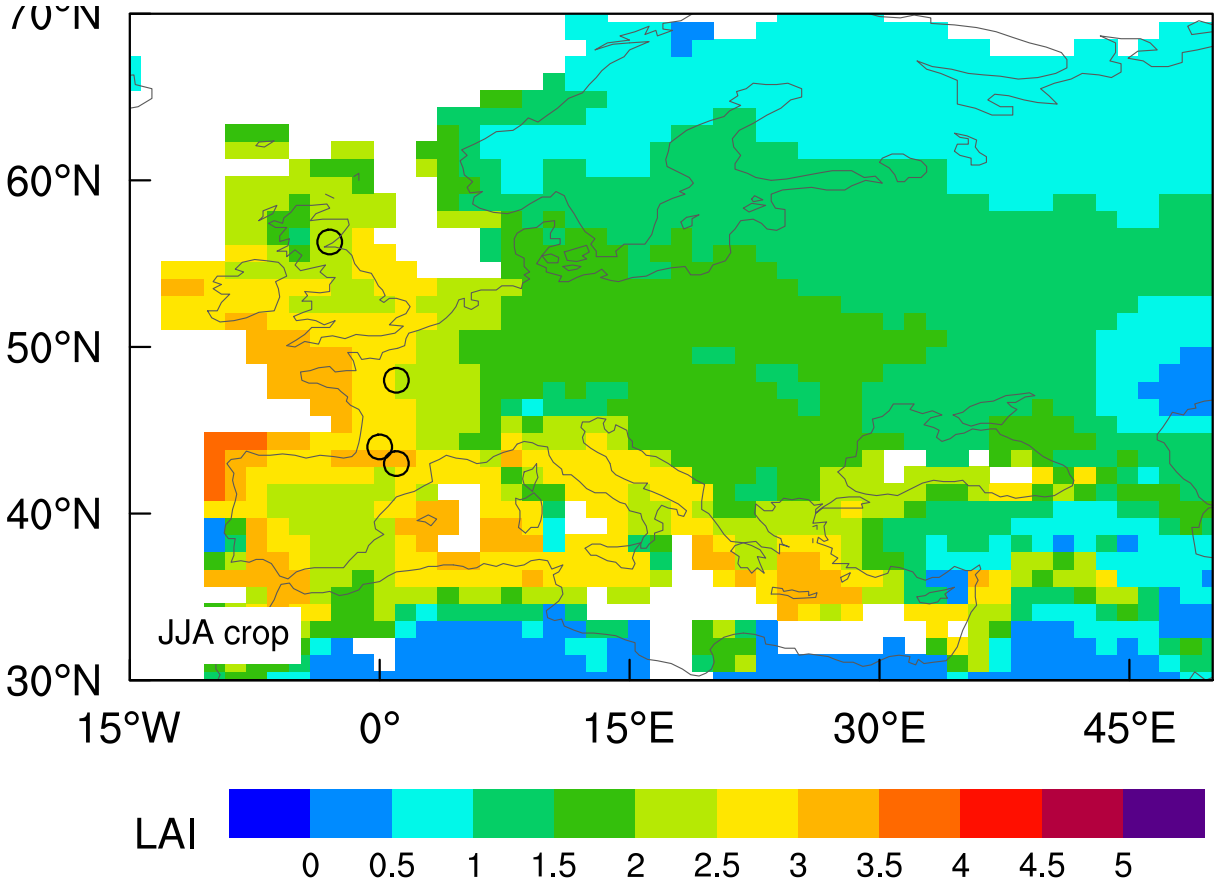

Figure S3. Spatial distribution of June-July-August LAI for croplands in LM4.0 (1990-2014).

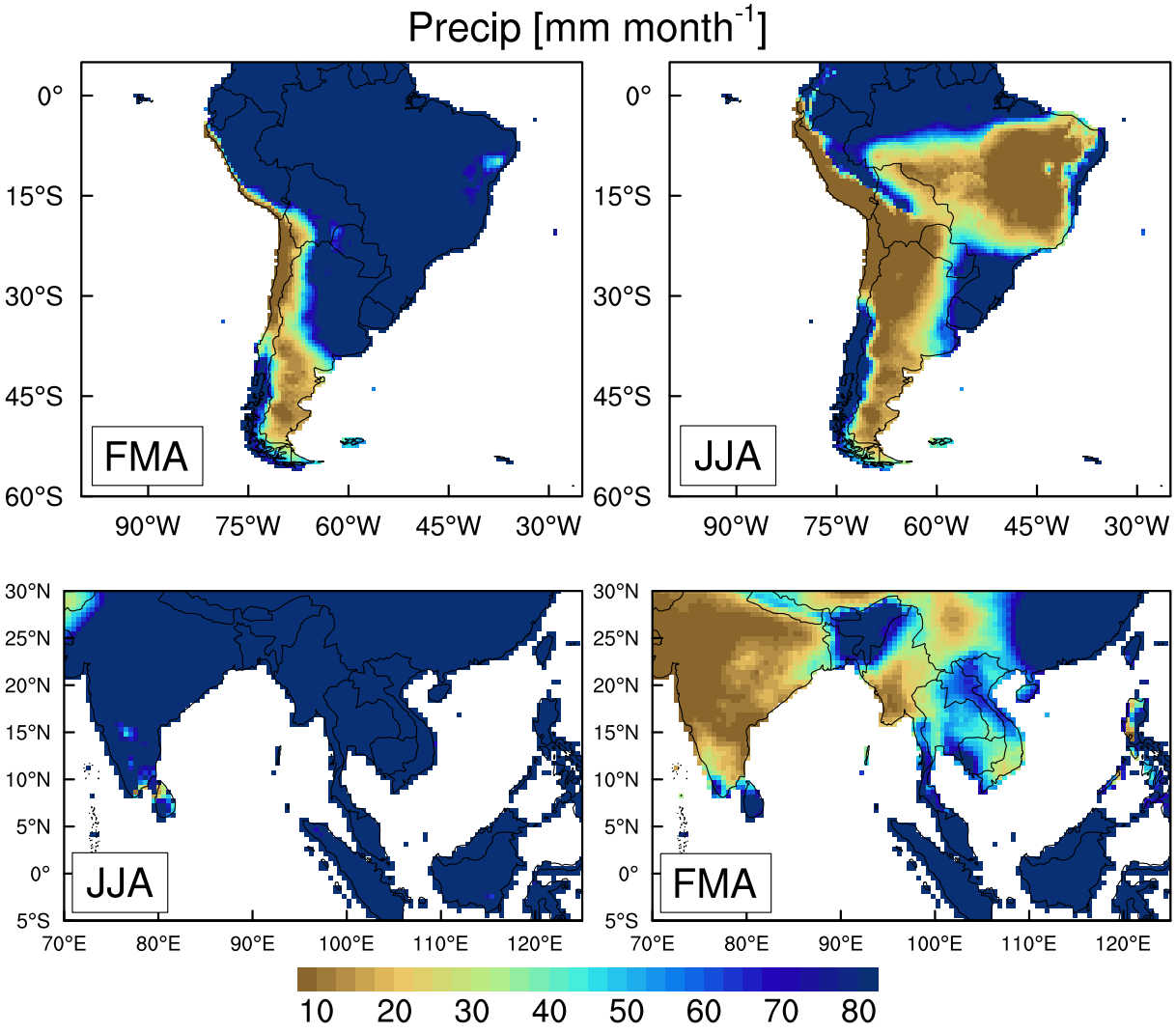

Figure S4. Comparisons of observed precipitation (CRU4.01) in the wet versus dry season over Amazon and over South Asia.

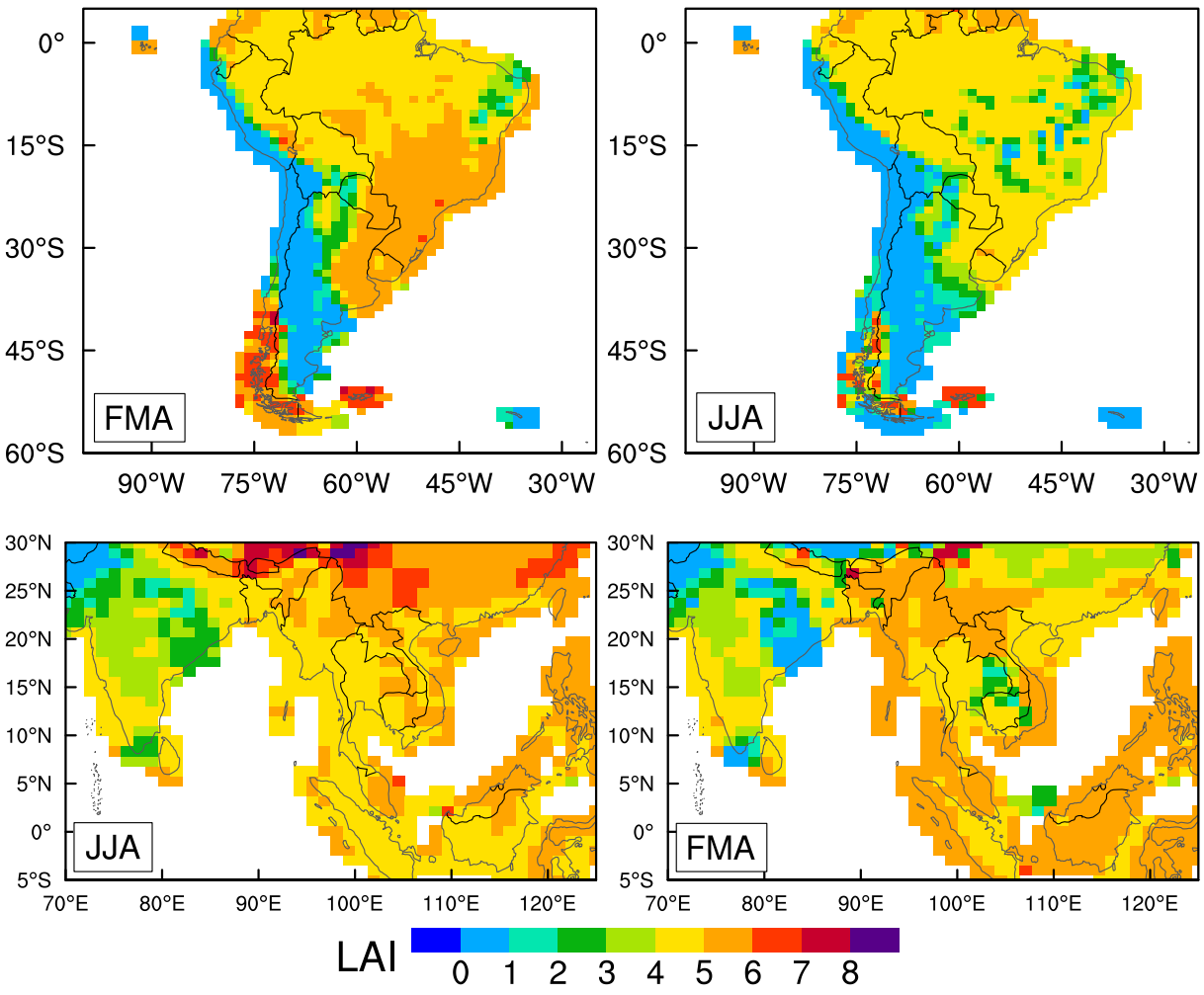

Figure S5. LM4.0 modeled LAI in the wet versus dry season for tropical evergreen forests in Amazon and in South Asia.

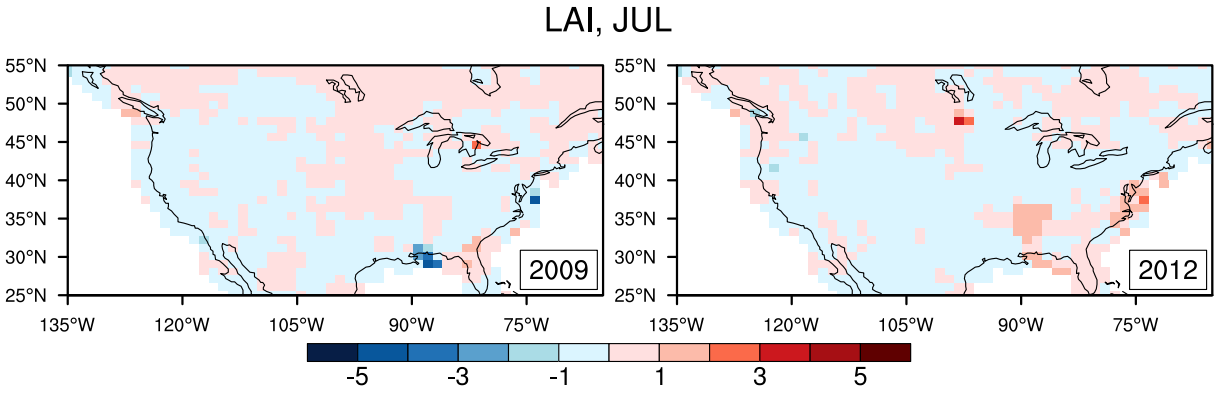

Figure S6. Little change in LM4.0 modeled LAI in July 2012 (dry) versus July 2009 (wet). Shown are anomalies relative to the 25-year (1990-2014) climatology.

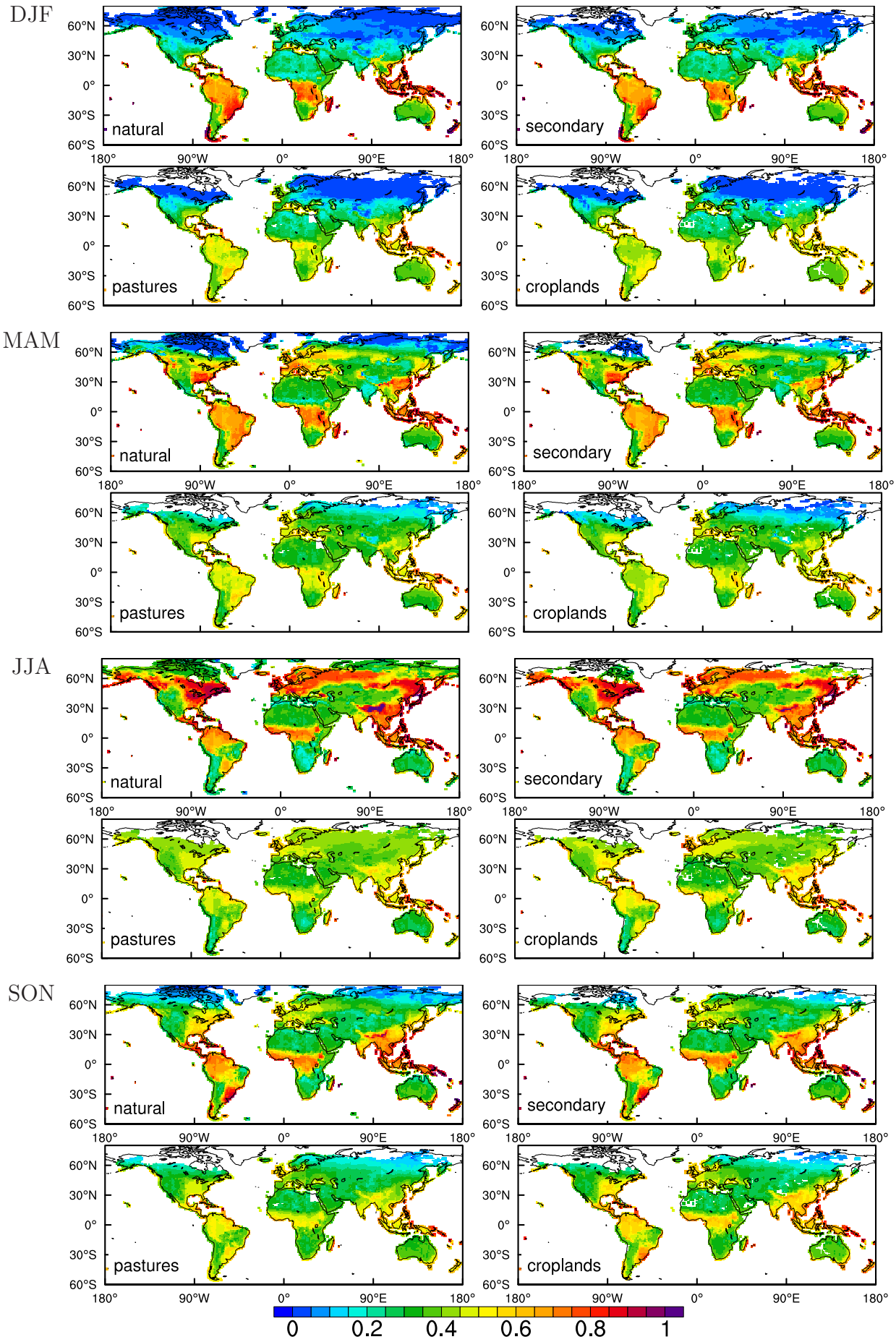

Figure S7. Global distributions of daytime (9am-3pm LT) mean $V_{d,O3}$ (in cm s^{-1}) to four landuse categories in LM4.0 for DJF, MAM, JJA, and SON averaged over the 1990-2014 period.

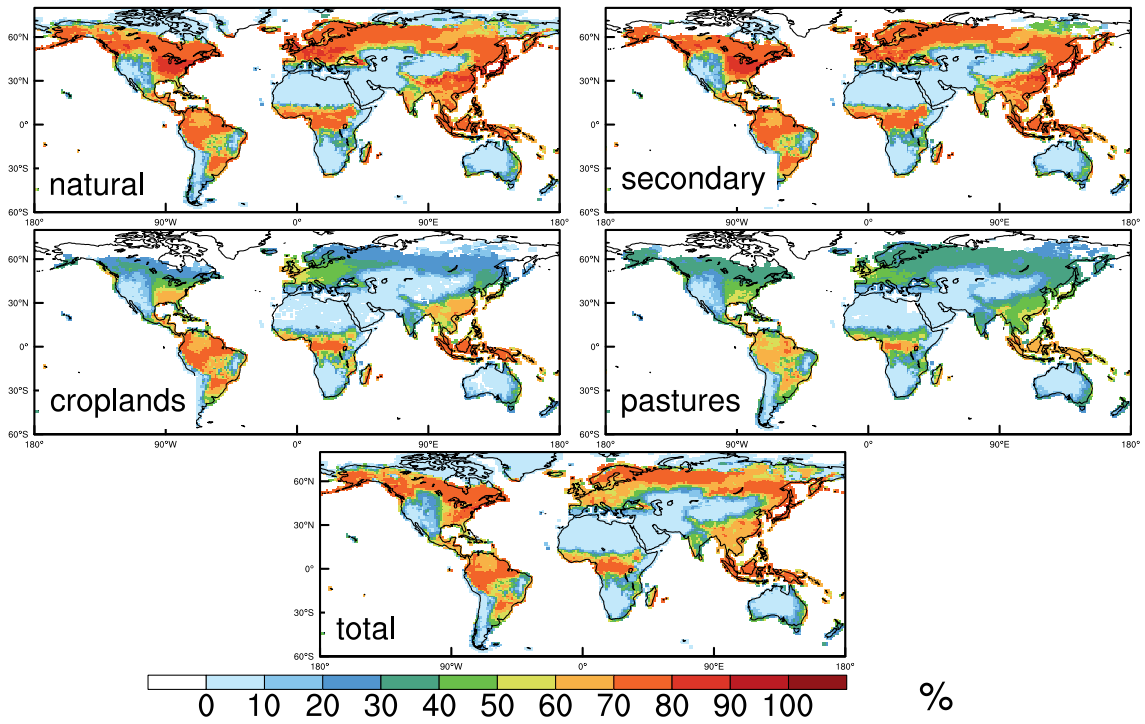

Figure S8. Global distributions of JJA daytime (9am-3pm LT) mean contribution of stomatal pathways to total $V_{d,O3}$ for four landuse categories in LM4.0. The 25-year climatology (1990-2014) is shown.

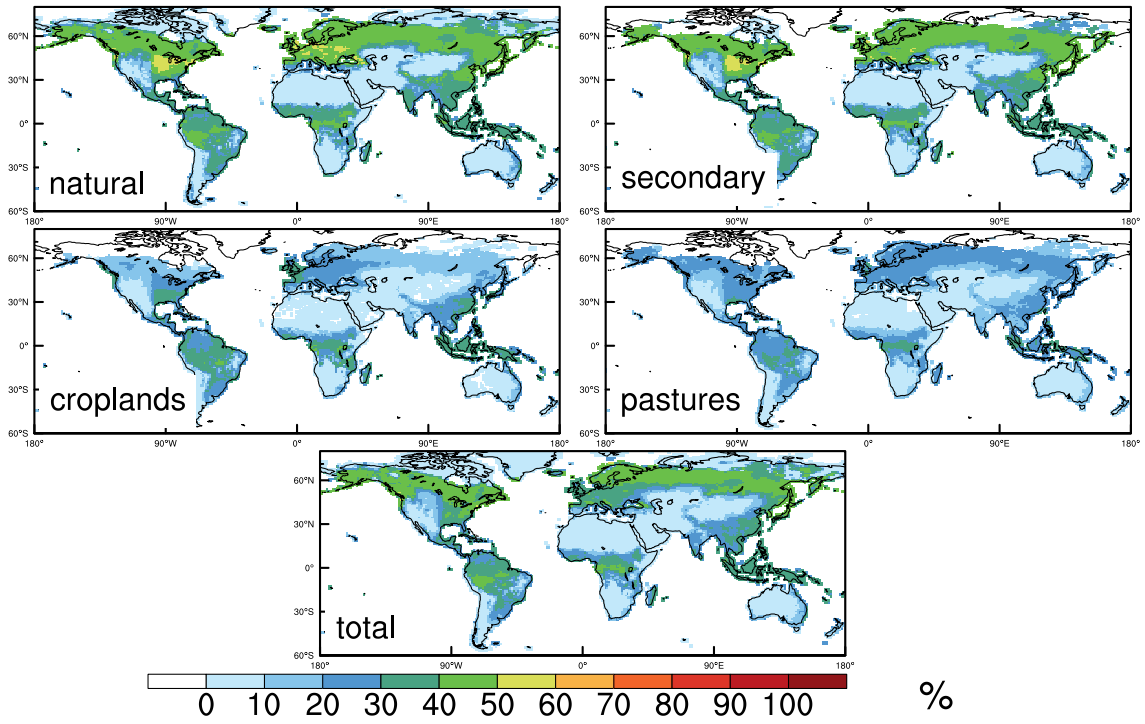

Figure S9. Global distributions of JJA 24-hour average contribution of stomatal pathways to total $V_{d,O3}$ for four landuse categories in LM4.0.